Carrier transfer effect on transport in *p-i-n* structures with Ge quantum dots

V. S. Lysenko, Yu. V. Gomeniuk, V. V. Strelchuk, and A. S. Nikolenko
Institute of Semiconductor Physics, 41 Prospect Nauki, UA-03028, Kiev, Ukraine

S. V. Kondratenko*
Kiev National Taras Shevchenko University, Physics Department, 2 Acad. Glushkov Ave, UA-03022, Kiev, Ukraine

Yu. N. Kozyrev and M. Yu. Rubezhanska
O. O. Chuiko Institute of Surface Chemistry, 17 Generala Naumova Str., 03164, Kiev, Ukraine

C. Teichert
Institute of Physics, Montanuniversitaet Leoben, Franz Josef Str. 18, A-8700 Leoben, Austria
(Received 1 February 2011; revised manuscript received 17 May 2011; published 19 September 2011)

Coulomb charge accumulation and carrier transfer by valence band states of Ge quantum dots (QDs) embedded in the intrinsic region of Si *p-i-n* structures are studied by admittance and photocurrent spectroscopy, capacitance–voltage techniques, and Raman investigations. The effect of hole accumulation on the shape of direct current–voltage characteristics was found at temperatures <200 K. A blockade of conductivity via wetting layer (WL) states due to a positive charge trapped in QDs was observed. The effect was explained by thermally activated charge carrier transfer between QD and WL states.

DOI: 10.1103/PhysRevB.84.115425 PACS number(s): 72.20.Jv, 73.22.−f, 73.63.Hs

I. INTRODUCTION

Electric and optical properties of self-assembled quantum dots (QDs) are studied intensively because of their possible application to the design of nanoscale electronic devices.[1–3] The electronic structure of Ge QDs exhibits a type II band lineup with a large (∼0.6–0.7 eV) valence band offset, leading to hole confinement and the appearance of quantized energy levels.[4,5] In *p*-type Si-Ge multilayer structures, interlevel optical transitions between localized hole states in the midinfrared range[6,7] can be observed. The possibility of fabrication of photodetectors based on such subband transitions was demonstrated for Si-Ge quantum wells (QWs)[8,9] and QDs.[10–12]

QDs can be considered efficient traps for holes. Capture of positive charge carriers essentially influences transport, radiation efficiency, and nonradiative relaxation processes in Si-Ge structures.[13,14] It is commonly accepted that the carrier transfer between neighboring QDs occurs via the wetting layer (WL)[15,16] and that the luminescence of dots quenches due to carrier transfer between QD and WL states.[13] Transport in Si-Ge heterostructures with QDs largely depends on Coulomb blockade effects and charging effects. For a Schottky diode structure with Ge QDs embedded inside a Si depletion region, these effects were studied by electric methods such as capacitance–voltage measurements, deep-level transient spectroscopy, and admittance spectroscopy.[17–19]

In contrast to previous works,[5,17,20–22] here we applied the space charge spectroscopy technique to study the conductivity of reverse- and forward-biased *p-i-n* structures with Ge QDs embedded into an *i*-Si layer in the presence of a significant direct current (DC). Such structures are promising for the design of novel photodetectors and electroluminescent devices. In this respect, transport peculiarities, as well as charge accumulation and carrier transfer—caused by QD and WL states—should be studied carefully. The aims of this paper are to study the effect of hole capture on conductivity of *p-i-n* heterostructures with Ge QDs embedded into *i*-Si layer and to clarify the features of carrier transfer between the WL and the Ge islands. Our experimental study includes admittance, Raman, and photocurrent investigations for *p-i-n* structures with Ge islands grown by a molecular beam epitaxy (MBE) technique.

II. EXPERIMENT

Multilayer Si-Ge heterostructures were grown using an MBE technique on boron-doped ($\rho = 7.5\ \Omega\cdot$cm) *p*-Si(100) substrates. First, a 100-nm-thick buffer silicon layer was grown on the substrate with subsequent B doping up to 10^{18} cm^{-3}. After that, a five-period heterostructure with Ge QDs layers separated by Si spacers was deposited at 500 °C. The deposition rate was 1.0 nm/min for Si and 0.6 nm/min for Ge. After QD deposition, a Si spacer was grown until a high-contrast Si(100)2 × 1 electron diffraction image, which is typical for a smooth Si surface, was observed. The thickness of each Si spacer layer was ∼15 nm. The top QD layer was covered by a 20-nm-thick Si layer doped by Sb to 10^{18} cm^{-3}. In such a way, the *p-i-n* structures with Ge QDs embedded into the intrinsic Si region were grown. The layout of the multilayered heterostructure is shown in Fig. 1.

Sizes and surface densities of the QDs were controlled using atomic force microscopy (AFM) by scanning uncovered Si-Ge structures grown at the same conditions. AFM measurements were performed with an NT-MDT Ntegra microscope in semicontact tapping mode using Si cantilevers with a tip apex radius of ∼10 nm. The structures investigated were found to have bimodal size distribution reflecting a dense array of hut-clusters[23] plus scarce dome-shaped islands.[24] The average height of the hut-clusters was found to be 2 nm; the average edge size of the hut-clusters is a base of 24 nm with a dispersion of size of ∼20%. The surface density of the hut-clusters

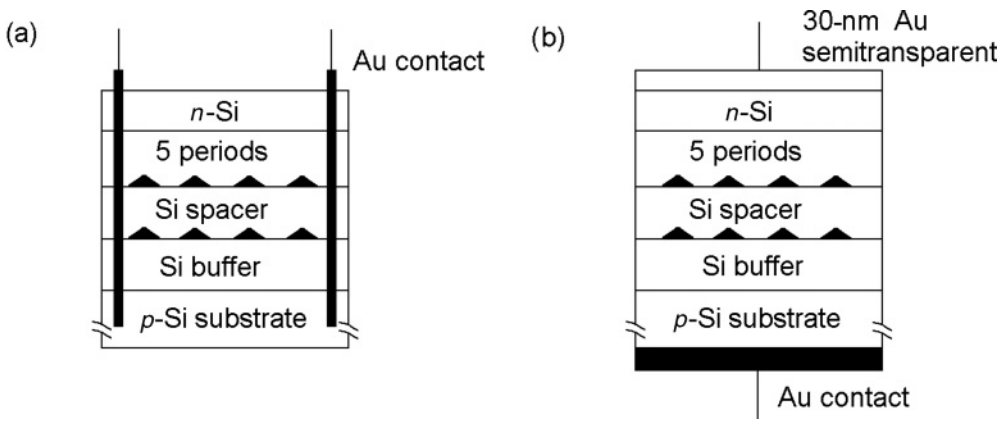

FIG. 1. Schematic view of multilayered Ge/Si heterostructure for measuring (a) lateral and (b) transverse photoconductivity and photovoltage.

was found to be 5×10^{10} cm^{-2}. The average height of the dome-shaped islands was ~12 nm, the base diameter was ~70 nm, and the surface density was $\sim 10^8$ cm^{-2}.

Admittance spectroscopy measurements were performed within a temperature range of 120–300 K under different bias voltages with an Agilent 4284 inductance–capacitance–resistance meter at frequencies of 100, 30 and 10 kHz. A Keithley 6485 picoammeter was used for DC–voltage measurements. Conductance, capacitance, and lateral photocurrent measurements were performed on *p-i-n* structures with a nontransparent Au back contact and 30-nm-thick semitransparent conducting Au film on the top Si layer [Fig. 1(b)].

Ohmic Au-Si contacts of rectangular shape and dimensions of 4×1 mm were welded into epitaxial layers at 370 °C for lateral photoconductivity measurements. The distance between contacts on the sample surface was 5 mm. Current–voltage (*I-V*) characteristics of the structures studied were found to be linear, in the range from −10 to +10 V, at temperatures between 77 and 290 K. Lateral photoconductivity spectra were measured at excitation energies ranging from 0.6 to 2.0 eV under illumination of a 250-W halogen lamp. The corresponding photocurrent signal was registered by a lock-in amplification technique with a modulation frequency of 80 Hz. Spectral dependences were normalized to the constant number of exciting quanta using a nonselective pyroelectric detector.

Micro-Raman spectra were recorded at room temperature using a computer-controlled Raman diffraction spectrometer (T-64000 Horiba Jobin-Yvon) with a cooled charge-coupled device detector. Excitation was performed with a 488-nm line of a Ar-Kr ion laser that had a power of 3 mW. Micro-Raman spectra were measured in $z(x,y) - x$ geometry, where the x, y, and z axes correspond to the crystallographic directions [100], [010], and [001], respectively. The radiation was focused by an Olympus long-focus objective, 50× magnification, 0.5 numerical aperture lens. Such geometry was chosen because it allows for scattering on longitudinal optical phonons in germanium and silicon, whereas two-phonon scattering on transverse acoustic phonons in the Si substrate is forbidden. This setup avoids complications in the interpretation of the Raman spectra.[25,26]

III. RESULTS AND DISCUSSION

A. Raman spectroscopy

The composition and values of elastic strains in the investigated Si-Ge heterostructures were analyzed using Raman spectroscopy. The obtained Raman spectrum (Fig. 2) reveals a three-mode behavior with phonon bands corresponding to Ge-Ge, Si-Ge, and Si-Si vibrations, which is typical for Si-Ge heterostructures with nanoislands.[27–31] Doublet behavior of the phonon bands, which is especially apparent for Ge-Ge and Si-Ge modes, evidences the existence of two types of $Si_{1-x}Ge_x$ solid solutions with different composition or elastic strains. Generally, for Si-Ge heterostructures with nanoislands, this effect can be attributed to a nonuniform island structure[32] or to their bimodal size and shape distributions.[27,28] A rather high growth temperature of the investigated structures (500 °C) allows us to rule out the first possibility due to strong interdiffusion processes observed in such heterostructures.[2] Another possible reason for the doublet band behavior could be scattering in the WL or Si/Ge interface, but the contribution of these regions to Raman spectra was shown to be negligible and is manifested only as line broadening.[33] As mentioned in the experiment section, the nanoislands investigated exhibit

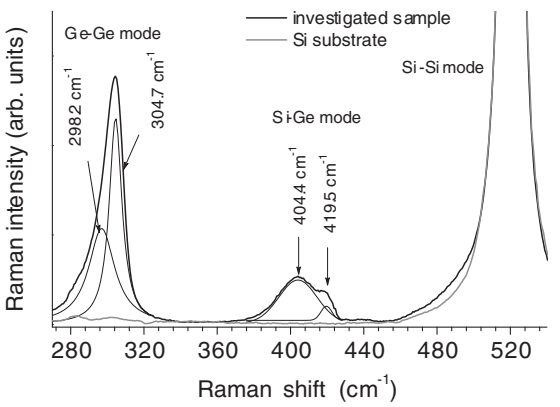

FIG. 2. Raman spectrum of a five-period Si-Ge heterostructure with a SiGe QDs of ~2 nm in height. The dashed line shows the Raman spectrum of the Si substrate for comparison. The layout of the experiment is $z(x,y) - z$. $\lambda_{excit} = 488$ nm, and T = 300 K.

a bimodal size distribution with small hut-clusters (average height of ~2 nm) and dome-shaped islands (average height of ~12 nm). This allows us to consider the observed doublet band behavior to be related to contributions of different types of SiGe nanoislands.[27,28]

The observed doublet Ge-Ge and Si-Ge phonon bands were decomposed into Lorentz lines with maxima at 298.2 and 304.7 cm^{-1} for Ge-Ge, as well as maxima at 404.4 and 419.5 cm^{-1} for Si-Ge modes (Fig. 2). The frequency positions of Si-Ge and Ge-Ge modes for a strained $Si_{1-x}Ge_x$ solid solution can be described as follows[29,30]:

$$\omega_{\mathrm{Si-Ge}} = 400 + 29x - 95x^2 + 213x^3 - 170x^4 - b_s\varepsilon_{xx} \quad (1)$$

$$\omega_{\mathrm{Ge-Ge}} = 282.5 + 16x - b_s\varepsilon_{xx}, \quad (2)$$

where b_s is the phonon deformation potential with the composition dependence

$$b_s = b_4(x-1)^4 + b_0, \quad (3)$$

with $b_4 = -190$ cm^{-1} and $b_0 = -400$ and -575 cm^{-1} for Ge-Ge and Si-Ge bands, respectively.[31] Using frequency positions of Ge-Ge and Si-Ge phonon bands and Eqs. (1)–(3), we determined composition and values of elastic strain for each type of $Si_{1-x}Ge_x$ nanoislands. Thus, the Ge content and elastic strains in hut-clusters were found to be $x = 0.87$ and $\varepsilon_{xx} = 0.016$. For the dome-shaped nanoislands, these values are $x = 0.46$ and $\varepsilon_{xx} = 0.023$. Taking into account the low density of dome islands and an essentially lower conductivity of silicon-enriched islands, we suggest that their effect on the total conductivity of the system is negligible.

B. Band diagram and photocurrent spectrum of Si-Ge heterostructures with QDs

The band diagram of the investigated Si-Ge nanosized heterostructures was calculated using Nextnano 3 software,[34] as well as data on composition and elastic strain in nanoislands obtained from Raman spectra analysis. Scare dome-shaped $Si_{0.54}Ge_{0.46}$ islands with lower Ge content can produce an observable Raman signal. However, this has no essential effect on the carrier transport and the photoconductivity. Therefore, the calculations were performed for structures with $Si_{0.13}Ge_{0.87}$ QDs. The obtained band diagram of the *p-i-n* heterostructure with $Si_{0.13}Ge_{0.87}$ QDs is shown in Fig. 3. The depths of the potential wells for heavy and light holes were found to be 0.73 and 0.6 eV, respectively. Therefore, holes are effectively localized in QDs. Quantization of the hole in Ge QDs leads to appearance of two localized states in the valence band. The energy gaps between the states of the QD valence band and the bottom states of the WL conduction band were found to be 0.6 and ~1.0 eV for ground and excited states, correspondingly. The activation energy of the ground and excited states for heavy holes appeared to be 0.44 and 0.15 eV, respectively.

To determine experimentally the energies of band-to-band transitions with participation of QD valence band states, we employed the spectroscopy of lateral photoconductivity, which previously was successfully used for determination of electronic spectrum of Si-Ge heteronanostructures.[35–38] In this case, the applied voltages have no effect on the obtained energy values due to lateral geometry. Interband optical transitions in QD and WL are responsible for the appearance of photocurrent at 77 K in the range of $h\nu < 1.04$ eV, in which single-crystalline silicon is transparent. This threshold energy for observation of interband optical transitions in *c*-Si is slightly lower than the band gap at a given temperature (1.17 eV at 77 K). This is because the contribution into the lateral photoconductivity of ~1.04 eV is determined by the absorption in the deformed silicon surrounding the nanoislands.[35] The decrease of the lateral photocurrent beyond 1.2 eV is caused by a high rate (>10^5 cm/s) of surface recombination,[39] because QDs act as effective recombination centers for electron-hole pairs photoexcited in *c*-Si.

The lateral photocurrent spectrum presented in Fig. 4 was found to agree well with the calculated energy diagram. From the photoconductivity spectrum plotted in $\ln(I_{PC})$ vs $h\nu$ coordinates, it is possible to distinguish a few components with threshold energies of 0.63 and 0.88 eV. Electron-hole pairs generated in the result of optical transitions involving localized states of nanoislands and the WL contribute to lateral photoconductivity in the range of $0.63 < h\nu < 1.04$ eV. The component of photocurrent with the threshold energy $h\nu = 0.63$ eV corresponds to an indirect electronic transition from the ground state of the nanoisland's valence band to the conduction band of the surrounding silicon. Above $h\nu = 0.88$ eV, the photocurrent is determined by transitions involving the excited states of nanoisland valence band and, with further increase of $h\nu$, by the interband transitions in

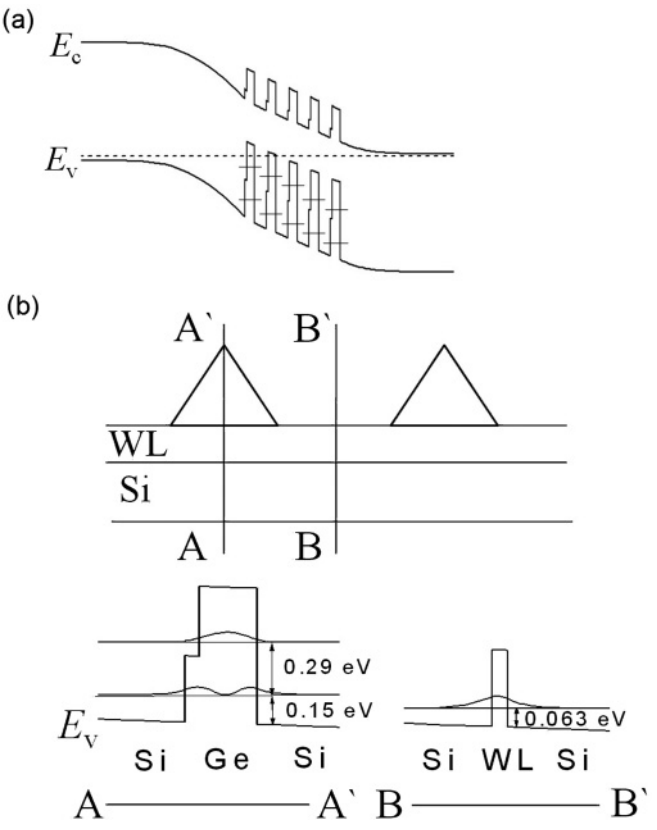

FIG. 3. (a) Energy diagram of unbiased *p-i-n* heterostructures with QDs. (b) Schematic of the valence band in the AA′ and BB′ directions.

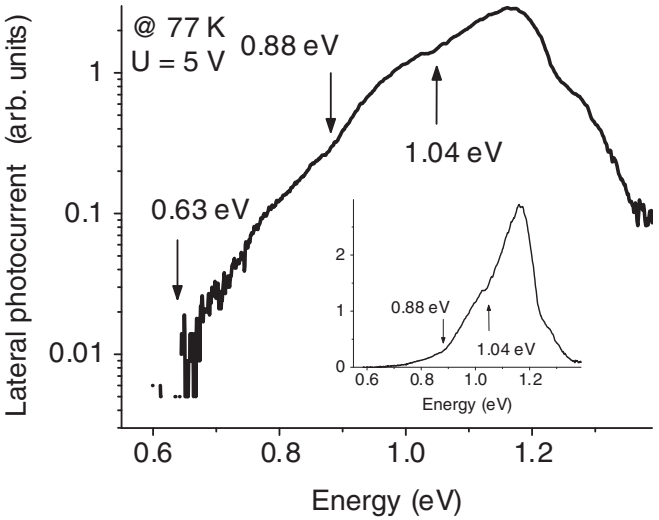

FIG. 4. Spectral dependence of the lateral photoconductivity (logarithmic scale) of Si-Ge heterostructures containing five layers of 2-nm-high Ge nanoislands. The inset shows the lateral photocurrent in linear presentation.

WL. Taking the observed characteristic energies of optical transitions into account, we estimate the activation energies for the hole ground state as $1.04 - 0.63 = 0.41$ eV and for the first excited state of the nanoisland as $1.04 - 0.88 = 0.16$ eV.[37,38]

C. *I-V* dependences and Coulomb charging effect

Figure 5 presents *I-V* dependences of *p-i-n* heterostructure with Ge QDs at different temperatures. In case of negative voltage applied to the n^+ Si layer ($V < 0$), the structure is forward biased. The *I-V* characteristics were recorded from the forward bias of -1.0 V to the reverse bias of $+2.0$ V with the sweep rate of 0.067 V/s. The *I-V* curves shift to the negative voltages with lowering of the temperature. For example, the shift was $\sim$0.2 V at 180 K. These results indicate a positive charge accumulated by QDs in the *i*-layer.

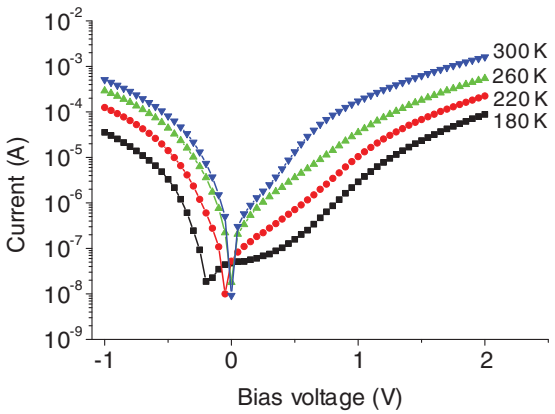

FIG. 5. (Color online) *I-V* characteristic of the structure as a function of the temperature. From bottom to top, the temperatures are 180, 220, 260, and 300 K. The plateau from -0.2 to $+0.5$ V and the shift of the curve at 180 K are due to the trapping of positive charges.

The forward current density at the injection levels chosen in the experiment is limited by the recombination rate of electrons and holes in the intrinsic region of the *p-i-n* structure.[39] In our case, the recombination centers are SiGe QD and WL states embedded into the *i*-Si layer. The recombination processes in the space charge region are mainly determined by the holes trapped at localized states in the valence band. At low temperatures, QD and WL states can accumulate positive charges that limit the forward current due to the increase of the recombination rate via QD and WL states. The increase of the forward current occurs with the temperature increase due to decreasing the charge trapped at the levels of QDs and WL. This recombination mechanism is considered in more detail in Sec. III D.

The reverse branch of the *I-V* curve exhibits at 180 K a plateau in the range from -0.2 to $+0.5$ V with a very weak dependence of current (or DC conductance) on bias voltage due to release of the trapped positive charge. Accumulation of the positive space charge by QDs (hole traps) during their charging by forward current leads to a change of the electric field in the depletion region and to an appearance of an additional static resistance R_{st}, because the hole current J_h through the *p-i-n* structure is limited at low temperature. The magnitude of this resistance increases with the temperature decrease and can be estimated as $R_{st} = \Delta V / J_h = 4 \times 10^8\ \Omega$ at 180 K, where $\Delta V = 0.2$ V represents the voltage range with a constant DC. In this case, the supply of carriers from contacts is blocked by Coulomb charges accumulated in the QDs. This leads to the essential reduction of dark currents, which is <100 pA at 77 K. Such low dark currents can provide a high detection ability of photodetectors.

The current density at low reverse bias ($V < 1.0$ V) of the *p-i-n* structure depends on an effective thermal emission of holes from the states in the valence band of QDs and the WL. The density of the hole emission current from the QW states is given by

$$J_e = e_T \cdot n_{2D}, \tag{4}$$

where e_T is the thermal emission rate and n_{2D} is the two-dimensional hole concentration in the QW. Because the quantization in the considered Ge nanoislands takes place only in the growth direction, the temperature dependence of the

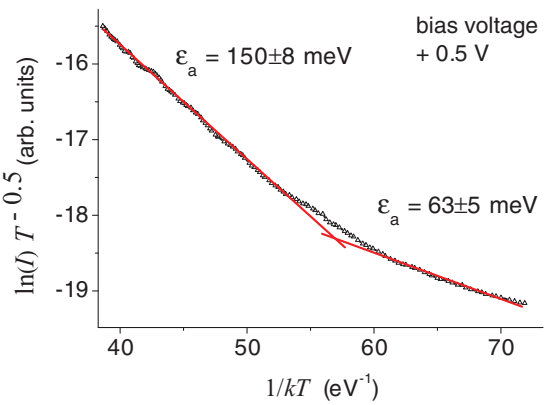

FIG. 6. (Color online) Temperature dependences of the current at an applied reverse bias $V = +0.5$ V.

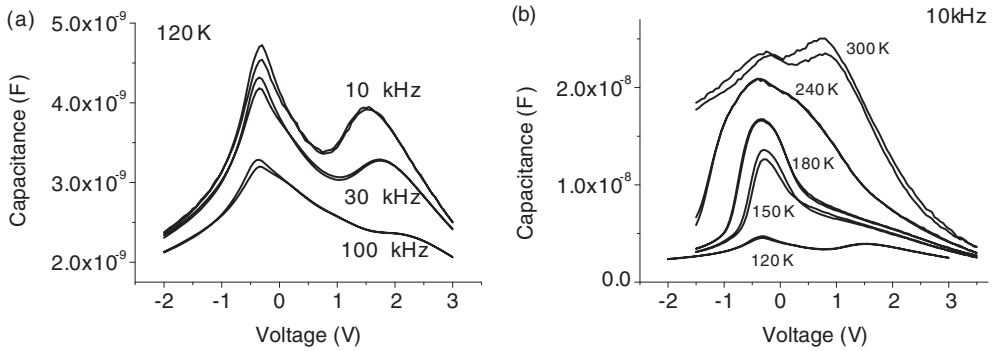

FIG. 7. (a) Capacitance–voltage dependences of *p-i-n* heterostructures recorded at different frequencies: 10, 30, and 100 kHz. (b) Capacitance–voltage dependences at different temperatures recorded at a modulation frequency of 10 kHz.

system's conductivity can be described by the equation typical for QW,

$$J_e(T) \sim T^{1/2} \exp\left(-\frac{E_a}{kT}\right), \tag{5}$$

where $E_a = E_i - E_v$ is the activation energy from the QD level E_i, closest to the top of the valence band of the surrounding Si.

The activation energy can be obtained from the slope of the Arrhenius plot of the current temperature dependence $\ln(I) \cdot T^{-0.5}$ vs $1/kT$, as has been performed in Fig. 6. At low biases, the complex temperature dependence of the dark current was observed with two activation energies of 63 and 150 meV. The value of 150 meV corresponds to thermal emission from the QD level closest to the Si valence band edge. This value agrees well with the calculated value of the activation energy for the first excited level. The activation energy of 63 meV corresponds to the thermal emission from the valence band states of the WL to delocalized states of the surrounding Si. The obtained experimental values of activation energy might be underestimated as compared to the binding energy values due to the field-dependence effect.

With the increase of the reverse bias, probably, the mechanism controlling the carrier transport changes from thermal emission to tunneling. At $V > 1.0$ V, *I-V* characteristics are fitted by the equation—which is typical for heterostructures—where the reverse current does not saturate and increases exponentially with applied bias,[39]

$$J_e \sim \exp\left(\frac{V}{V_0}\right) \exp\left(\frac{T}{T_0}\right), \tag{6}$$

where $T_0 = 40 \pm 2$ K and $V_0 = 0.53 \pm 0.01$ V.

D. Alternate current conductance and capacitance behavior

The effect of accumulated positive charge in the QDs on carrier transport in the *p-i-n* structure was studied by investigation of frequency and field dependences of conductivity and capacitance at different temperatures. In conductance–voltage and capacitance–voltage measurements, the applied voltage was swept from the forward (negative at the top electrode) bias $V = -2.0$ V to the reverse (positive) bias $V = +3.0$ V. In case of essential leakage currents, the results of both *G-V* and *G-ω* measurements require corrections, as described in Ref. 40. Before the conductance is plotted in G/ω vs frequency or voltage coordinates, the DC conductance should be subtracted from the measured value. The DC conductance G_{DC} was obtained experimentally from *I-V* curves.

Figure 7 shows the capacitance–voltage dependences measured at frequencies of 10, 30, and 100 kHz for temperatures between 120 and 300 K. Two peaks located at $V = -0.3$ V and near $V = 1.6$ V are observed in the *C-V* curves recorded at 120 K [Fig. 7(a)]. The temperature increase leads to a gradual shift of the second peak to lower voltages at temperatures $<$ 240 K [Fig. 7(b)], whereas the position of the peak at $V = -0.3$ V practically did not change.

Temperature-dependent alternate current (AC) conductance–voltage measurements were carried out at frequencies of 10, 30, and 100 kHz. The obtained *G-V* characteristics agree with the results of *C-V* measurements, showing the similar temperature dependence of two conductance peaks (at -0.3 V and $+1.3$ V) (Fig. 8). The frequency increase up to 100 kHz made it possible to more clearly separate the contribution of QD states to conductivity.

The constant position of the AC conductance peak at small forward bias indicates that the Fermi level is almost pinned and that the electric field is effectively screened by the accumulated positive charge. In the case of *p-i-n* heterostructures with Ge QDs embedded into *i*-Si layer, the conductance at small applied voltages is dominated by the lowest potential barriers in the region with epitaxial layers. Thus, the peak at small forward bias is related apparently to the WL. The peak at

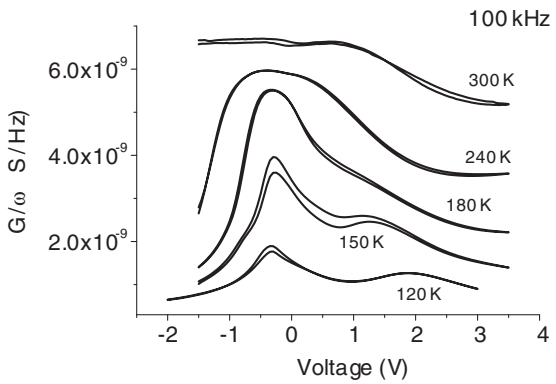

FIG. 8. Conductance–voltage characteristics measured at a modulation frequency of 100 kHz at different temperatures.

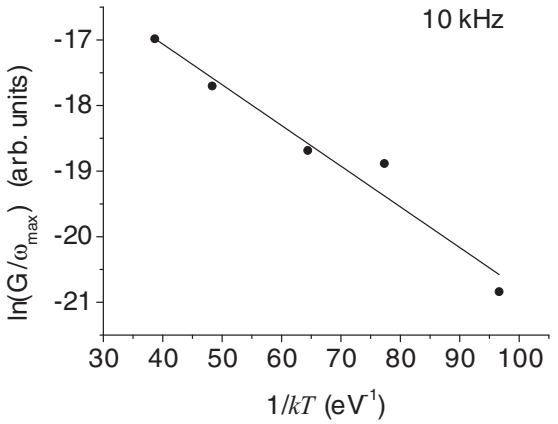

FIG. 9. Arrhenius plot of $G/\omega_{\max}$ of the conductance peak observed near $V = -0.3$ V at different temperatures at 10 kHz.

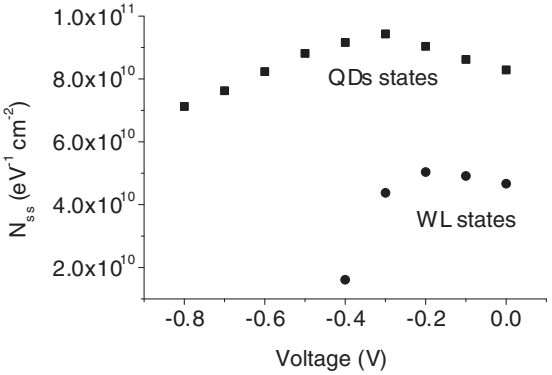

FIG. 11. Density of states in QD and WL contributing to conduction, as a function of applied forward voltage at 120 K.

reverse biases shifts toward lower voltages with increasing temperature due to QD recharging. At temperatures >180 K, both peaks overlap. The peak at reverse bias, when the QDs are in the depletion layer, is due to recharging of the deeper QD states. A gradual shift of the second peak to lower voltages can be explained by a temperature-field dependence of the binding energy of holes localized at QD states. Such behavior is typical for heterostructures with QDs, where thermally activated tunneling via a potential barrier can decrease the activation energy.[5,21]

The activation energy is estimated from measurements of G/ω peak value at 10 kHz around $V = -0.3$ V for different temperatures. In Fig. 9, a corresponding Arrhenius plot of $G/\omega_{\max}$ of the conductance peak is shown, yielding an activation energy of 62 meV. The temperature dependence of the AC conductance for the Si/Ge/Si heterostructures with QDs is determined by the lowest potential barrier of the WL. The obtained value of the activation energy corresponds to the thermal emission from the WL valence band states to the states of the surrounding Si. It agrees with the value of 63 meV obtained from the analysis of the temperature dependences of the DC and with the results presented by Schmalz *et al.*[5,21]

At 300 K [see Fig. 7(b)], a peak in the C-V curve around +0.8 V was observed. This peak is probably related to the carrier generation from deeper states in the SiGe/Si interface.[14] At lower temperatures, these states are apparently filled and are not manifested in C-V and G-V measurements.

The effect of positive charge trapped at QD on the transport in p-i-n structure is also observed in conductance–frequency measurements. The frequency dependence of conductance at $V = 0$ V and $T = 120$ K shows two peaks (Fig. 10(a)), the first one ≈4 kHz and the second one ≈200 kHz. The low-frequency peak, which is related to recharging of the WL states, appears at low filling (low forward biases). The high-frequency conductance peak is related to recharging of deeper states in the QD valence band.

The frequency dependences were measured under conditions in which Ge nanoislands were situated in the depletion region of the p-i-n structure, which allowed use of the equivalent circuit consisting of barrier capacitance C_s, QD and WL capacitance C_{dot}, and total conductance of system G [Fig. 10(a) inset]. In this case, the analysis of frequency dependences of the conductance at given biases makes it possible to determine the characteristic recharging time of the QD and WL states and to determine the density of states contributing into the conductance.

As can be seen in Fig. 10(a), the G/ω vs ω dependence at 120 K has two maxima at $\omega_{\max} = \tau^{-1}$ giving the characteristic times of charge exchange of 8.6×10^{-7} and 4.0×10^{-5} s at zero voltage for QD and WL states, respectively. The value of $G(\omega)/\omega$ at the maximum equals to $C_s/2$, and the density of states can be estimated as $N_s = C_s/qA$, where A is the sample area.[39] QD density of states contributing to high-frequency conductance is $N_s = 8.3 \times 10^{10}$ cm^{-2} eV^{-1} at 0 V. As the forward bias increases, the Fermi level in the region with QDs

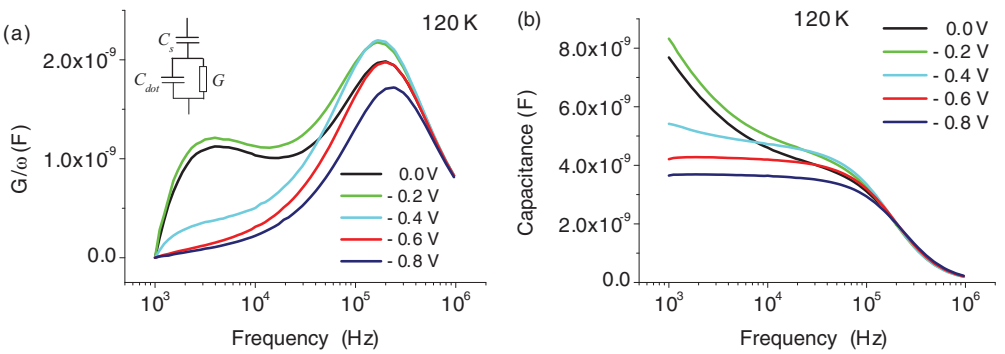

FIG. 10. (Color online) Frequency dependences of (a) conductance and (b) capacitance at different biases and $T = 120$ K. The inset in (a) shows the corresponding equivalent circuit.

moves down, corresponding to stronger filling with holes of QD and WL states (Fig. 11). At $V < -0.3$ V, conductance via QD states decreases with an increase in hole filling. At the same time, a sharp drop of the conductance via WL states is observed, i.e., there is a blockade of the system's conductance by the positive charge of QDs at low temperatures.

Lowering the temperature leads to essential modification in the shape of the capacitance frequency characteristics, as can be seen in the corresponding plot presented in Fig. 10(b). At full filling (large space charge, i.e., high resistance of the depletion region), the system capacitance is determined mainly by the capacitance of QDs situated in the space charge region. In this case, the capacitance does not depend on frequency in the range from 1 to 30 kHz and is equal to 3.7 nF. The capacitance of a disk-shaped QD of the diameter d, according to laws of classic electrostatics, is given by the equation $C_{\mathrm{QD}} = 4\varepsilon\varepsilon_0 d$. For $d = 20$ nm and $\varepsilon = \varepsilon_{\mathrm{Ge}} = 16$, we get the capacitance value $C_{\mathrm{QD}} = 7.9 \times 10^{-18}$ F. For the investigated set of dots with a surface density of $\sim 5 \times 10^{10}$ cm^{-2}, the capacitance is $C_0 \approx 4$ nF, which agrees well with the experimental value.

The system's capacitance saturates with the increase of the forward bias in the range of $V < -0.5$ V, as the QD states are being filled with holes. This is explained by Fermi level pinning, i.e., by a weak shift with an increase of the forward bias.

The amount of charge captured by dots can be estimated using the plateau range $\Delta V = 0.2$ V at low-temperature DC–voltage dependence as $Q = C_0 \cdot \Delta V = 0.74 \times 10^{-18}$ C, which corresponds to the capture of one hole by the QD. Because Coulomb blockade effects can be observed under the condition $C_{\mathrm{QD}} < \frac{e^2}{2kT}$, where C_{QD} is the capacitance of the QD ($C_{\mathrm{QD}} < 3.1 \times 10^{-18}$ F at 300 K), the effect of the charge state of the QD on charge carrier transport should be taken into account in the considered system.

The obtained results agree well with the model suggested in Refs. 5 and 21. As it was supposed in Refs. 5 and 21, based on the results of measurements using the space charge spectroscopy technique, the hole emission from nanoislands takes place via a two-step process. Hole emission from the nanoislands into the WL occurs at the first stage, and the second stage corresponds to an emission from the WL into the surrounding Si.

The merging of peaks with increasing temperature—as observed in the corresponding G-V dependences (see Fig. 8)—is caused by the coupling of WL states with the first excited QD state. The hole exchange rate between these states was found to essentially depend on temperature. The capture of holes by the QDs influences the rate of the hole exchange between QD and WL states. The density of positive charge increases at low temperatures, and such a carrier jump becomes less probable, which determines conductivity and capacitance of the whole system. This indicates that the localized states in the valence bands of QDs and WL at low temperature are separated by a relatively high potential barrier of the transition layer, which prevents the effective carrier exchange between states in the QDs and the WL.

The electric field of the barrier is determined by the positive charge of holes being accumulated in the nanoislands, preferably near the bottom,[41] and by electrons localized in the surrounding silicon. Assuming a higher density of localized states in the defect-rich transition layer of the WL around the bottom of the island, we expect a higher charge density in this region and the presence of a potential gradient in a lateral direction under the QD base.

The lateral electric field around the islands enhances the probability of hole tunneling into the WL.[5,21] Because the applied transverse electric field at the reverse bias has the same direction, it is enhancing hole tunneling from QD states into the WL. In this case, the system's conductance is determined by a tunnel-activation mechanism.

The change of frequency dependences of conductance [Fig. 12(a)] and capacitance [Fig. 12(b)] with increasing forward bias at higher temperature is different from that observed in low-temperature measurements. The conductance at 300 K increases because of lowering of the barrier at the forward bias and because of the absence of hole capture by QD and WL states. With increasing temperature, broadening of localized states of shallow QWs occurs. Consequently, the intensity of interchange between QD and WL states increases. The density of states equals to $N_s = 7 \times 10^{11}$ cm^{-2} eV^{-1} at $V = -0.1$ V.

In contrast to low-temperature measurements (see Fig. 9), at forward biases from -0.1 to -0.8 V and temperatures $T > 240$ K, the diffusion capacitance dominates the frequency dependence of the capacitance. The latter is described by the equation[39,42]

$$C = C_{\mathrm{geo}} + \frac{C_m}{1 + B\omega^s}, \tag{7}$$

where $s = 1.3$, C_{geo} is the geometric capacitance of sample, C_m is the temperature-dependent capacitance, and B is a

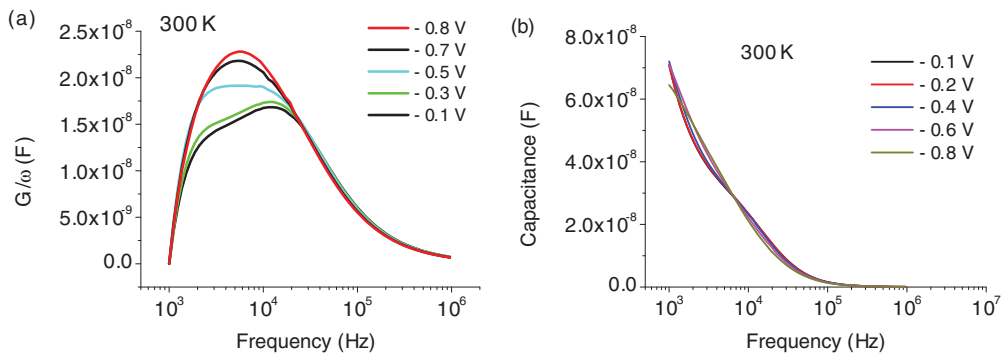

FIG. 12. (Color online) Frequency dependences of (a) conductance and (b) capacitance at different bias measured at 300 K.

constant. Thus, at high temperatures ($T > 240$ K), nanoislands behave as additional scattering centers and do not capture the positive charge.

IV. CONCLUSIONS

We demonstrated the effect of thermally activated charge transfer between QD and WL states in multilayer *p-i-n* structures containing SiGe QDs. A comparison between admittance spectroscopy and DC measurement shows that QDs capture holes at low temperatures. The Coulomb charge accumulated in the island affects the hole exchange rate between QD and WL states and determines the conductivity of the system at low temperatures. With temperature lowering, the trapped charge increases, resulting in a reduction of the hole exchange rate. The blockade of conductivity via WL states was observed when the QDs store a positive charge. Photocurrent spectra and admittance spectra were employed to verify an energy-level scheme of QDs. Measured activation energies and an interband energy gap are in good agreement with the calculated band diagram of Si-Ge heterojunction. The obtained results show the possibility of creating photodetectors that have a high sensitivity at low temperatures and are based on *p-i-n* structures with QDs.

ACKNOWLEDGMENTS

The research was implemented within bilateral Project No. UA 11/2009 of the Austrian Exchange Service and supported by the program of fundamental research of the National Academy of Sciences of Ukraine, Nanostructured Systems, Nanomaterials, Nanotechnologies, through Project No. 9/07 and by the Ministry of Education and Science of Ukraine through Project No. M/34-09.

*kondr@univ.kiev.ua

[1] O. G. Schmidt and K. Eberl, Phys. Rev. B **61**, 13721 (2000).
[2] K. Brunner, Rep. Prog. Phys. **65**, 27 (2002).
[3] W. G. van der Wiel, S. De Franceschi, J. M. Elzerman, T. Fujisawa, S. Tarucha, and L. P. Kouwenhoven, Rev. Mod. Phys. **75**, 1 (2003).
[4] S. K. Zhang, H. J. Zhu, F. Lu, Z. M. Jiang, and X. Wang, Phys. Rev. Lett. **80**, 3340 (1998).
[5] K. Schmalz, I. N. Yassievich, P. Schittenhelm, and G. Abstreiter, Phys. Rev. B **60**, 1792 (1999).
[6] C. Miesner, O. Röthig, K. Brunner, and G. Abstreiter, Appl. Phys. Lett. **76**, 1027 (2000).
[7] J. L. Liu, W. G. Wu, A. Balandin, G. L. Jin, and K. L. Wang, Appl. Phys. Lett. **74**, 185 (1999).
[8] P. Kruck, M. Helm, T. Fromherz, G. Bauer, J. F. Nützel, and G. Abstreiter, Appl. Phys. Lett. **69**, 3372 (1996).
[9] J. S. Park, R. P. G. Karunasiri, and K. L. Wang, Appl. Phys. Lett. **61**, 681 (1992).
[10] N. Rapaport, E. Finkman, T. Brunhes, P. Boucaud, S. Sauvage, N. Yam, V. Le Tranh, and D. Bouchier, Appl. Phys. Lett. **77**, 3224 (2000).
[11] P. Boucaud, T. Brunhes, S. Sauvage, N. Yam, V. Le Thanh, D. Bouchier, N. Rappaport, and E. Finkman, Phys. Status Solidi B **224**, 233 (2001).
[12] S. Tong, J. L. Liu, J. Wan, and K. L. Wang, Appl. Phys. Lett. **80**, 1189 (2001).
[13] J. Wan, G. L. Jin, Z. M. Jiang, Y. H. Luo, J. L. Liu, and K. L. Wang, Appl. Phys. Lett. **78**, 1763 (2001).
[14] D. W. Kwak, C. J. Park, Y. H. Lee, W. S. Kim, and H. Y. Cho, Nanotechnology **20**, 055201 (2009).
[15] R. Leon, S. Fafard, P. G. Piva, S. Ruvimov, and Z. Liliental-Weber, Phys. Rev. B **58**, R4262 (1998).
[16] S. Fafard, D. Leonard, J. L. Merz, and P. M. Petroff, Appl. Phys. Lett. **65**, 1388 (1994).
[17] S. K. Zhang, H. J. Zhu, F. Lu, Z. M. Jiang, and X. Wang, Phys. Rev. Lett. **80**, 3340 (1998).
[18] A. I. Yakimov, C. J. Adkins, R. Boucher, A. V. Dvurechenskii, A. I. Nikiforov, O. P. Pchelyakov, and G. Biskupski, Phys. Rev. B **59**, 12598 (1999).
[19] F. Lu, S. Wang, H. Jung, Z. Zhu, and T. Yao, J. Appl. Phys. **81**, 2425 (1997).
[20] C. Miesner, T. Asperger, K. Brunner, and G. Abstreiter, Appl. Phys. Lett. **77**, 2704 (2000).
[21] K. Schmalz, I. N. Yassievich, H. Rücker, H. G. Grimmeiss, H. Frankenfeld, W. Mehr, H. J. Osten, P. Schley, and H. P. Zeindl, Phys. Rev. B **50**, 14287 (1994).
[22] H. Zhou, S. Huang, Y. Rao, Z. Jiang, and F. Lu, Solid State Commun. **125**, 161 (2003).
[23] Y.-W. Mo, D. E. Savage, B. S. Swartzentruber, and M. G. Lagally, Phys. Rev. Lett. **65**, 1020 (1990).
[24] G. Medeiros-Ribeiro, A. M. Bratkovski, T. I. Kamins, D. A. A. Ohlberg, and R. S. Williams, Science **279**, 353 (1998).
[25] A. V. Kolobov, J. Appl. Phys. **87**, 2926 (2000).
[26] A. V. Baranov, A. V. Fedorov, and T. S. Perova, Phys. Rev. B **73**, 075322 (2006).
[27] J. S. Reparaz, A. Bernardi, A. R. Goni, M. I. Alonso, and M. Garriga, Phys. Status Solidi B **56**, 1 (2009).
[28] A. Bernardi, M. I. Alonso, J. S. Reparaz, A. R. Goni, P. D. Lacharmoise, J. O. Osso, and M. Garriga, Nanotechnology **18**, 475401 (2007).
[29] S. F. Ren, W. Cheng, and P. Y. Yu, Phys. Rev. B **69**, 235327 (2004).
[30] M. I. Alonso, M. de la Calle, and J. O. Osso, J. Appl. Phys. **98**, 033530 (2005).
[31] J. S. Reparaz, A. Bernardi, and A. R. Goni, Appl. Phys. Lett. **92**, 081909 (2008).
[32] M. Y. Valakh, V. Yukhimchuk, V. M. Dzhagan, O. S. Lytvyn, A. G. Milekhin, A. I. Nikiforov, O. P. Pchelyakov, F. Alsina, and J. Pascual, Nanotechnology **16**, 1464 (2005).
[33] P. H. Tan, K. Brunner, D. Bougeard, and G. Abstreiter, Phys. Rev. B **68**, 125302 (2003).
[34] Nextnano 3. "Device simulation package" [http://www.nextnano.de/.](09 June 2011).
[35] S. V. Kondratenko, O. V. Vakulenko, Yu. N. Kozyrev, M. Y. Rubezhanska, A. S. Nikolenko, and S. L. Golovinskiy, Nanotechnology **18**, 185401 (2007).
[36] S. Tsong, J. L. Liu, J. Wan, and L. Kang, Appl. Phys. Lett. **80**, 1189 (2002).

[37]C. Meisner, O. Röthig, K. Brunner, and G. Abstreiter, Appl. Phys. Lett. **76**, 1027 (2000).
[38]A. B. Talochkin, I. B. Chistokhin, and V. A. Markov, Nanotechnology **20**, 175401 (2009).
[39]S. M. Sze, *Semiconductor Devices: Physics and Technology*, 2nd edition (John Wiley & Sons, New York, 1985, 2002).
[40]Y. Gomeniuk, A. Nazarov, A. Vovk, Y. Lu, O. Buiu, S. Hall, J. K. Efavi, and M. C. Lemme, Mater. Sci. Semicond. Process. **9**, 980 (2006).
[41]L. Li, S. Ketharanathan, J. Drucker, and M. R. McCartney, Appl. Phys. Lett. **94**, 232108 (2009).
[42]K. Wang, H. Chen, and W. Z. Shen, Phys. B **336**, 369 (2003).